ACS Catalysis

Research Article

pubs.acs.org/acscatalysis

In Situ X-ray Absorption Fine Structure Studies on the Effect of pH on Pt Electronic Density during Aqueous Phase Reforming of Glycerol

Ayman M. Karim,*[,†] Christopher Howard,[†] Benjamin Roberts,[†] Libor Kovarik,[†,‡] Liang Zhang,[†] David L. King,[†] and Yong Wang[†,§]

[†]Institute for Integrated Catalysis and [‡]Environmental Molecular Science Laboratory, Pacific Northwest National Laboratory, P.O. Box 999, Richland, Washington 99352, United States

[§]Department of Chemical Engineering, Washington State University, Pullman, Washington, United States

Supporting Information

ABSTRACT: In situ X-ray absorption spectroscopy (XAS) results on correlating the Pt local coordination and electronic structure with the Pt/C catalyst activity and selectivity during aqueous reforming of glycerol at different pH are reported. The results show that both low and high pH favor C−O cleavage over that of C−C. However, the selectivity toward C−O bond cleavage was higher under the acidic conditions. XANES measurements under reaction conditions showed that low pH increased the Pt electron density while the effect of basic conditions was minimal. ΔXANES was used to estimate the coverage of adsorbates under reaction conditions and the results suggest a change in the adsorbates coverage by the acidic conditions, resulting in higher electron density on Pt.

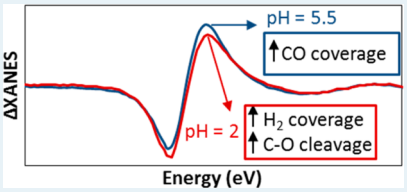

KEYWORDS: *In situ EXAFS, XANES, Pt/C, pH, aqueous phase reforming, adsorbates, electronic density*

INTRODUCTION

Because of the increase in energy demand and diminishing fossil fuels, it is necessary to develop new processes that use a sustainable resource such as lignocellulosic biomass[1] for the production of transportation fuels.[2,3] Several processes currently exist for the conversion of biomass to fuels including liquefaction,[4] fast pyrolysis/catalytic fast pyrolysis followed by hydrodeoxygenation or zeolite upgrading,[5−7] gasification followed by Fischer−Tropsch synthesis,[3] and aqueous phase conversion of carbohydrates.[2,8−13] Most of the aforementioned biomass conversion processes, especially the aqueous phase processing routes,[13] involve acidic liquids and precious metal catalysts at elevated pressures and temperatures, up to 55 bar and 400 °C.[13] To control the catalyst selectivity (C−C or C−O cleavage) under these conditions, it is necessary to understand how the aqueous phase, solution pH, and/or the identity of the acid or base affect the metal electronic structure and the reaction pathways.

Aqueous phase processing of biomass-derived products (e.g., sugars, bio-oil) is an important step in the conversion of biomass to fuels,[11−13] and understanding the effect of reaction conditions on the catalyst structure is crucial in developing better catalysts. However, only a few techniques can probe the catalyst structure in aqueous solutions at the elevated pressure and temperatures involved in biomass conversion processes. These techniques include: attenuated total reflection infrared spectroscopy (ATR-IR), X-ray absorption spectroscopy (XAS), and X-ray diffraction (XRD). Ebbesen at al. studied the effect of aqueous phase and pH on the CO chemisorption and CO oxidation rate on Pt/Al_2O_3 at room temperature using in situ ATR-IR and compared the results to that in the gas phase.[14] They showed that higher pH resulted in higher CO oxidation rate, and this correlated with a lower frequency of linearly adsorbed CO. They attributed the frequency shift of linearly adsorbed CO and dependence of CO oxidation rate on pH to a potential change of the metal.[14] In situ ATR-IR was also used recently by Wawrzetz et al. to identify some of the intermediates during aqueous phase reforming of glycerol on Pt/Al_2O_3 at 225 °C and 420 psig. It should be noted that the pH and temperature ranges for ATR-IR are limited by the ZnSe crystal. Dietrich et al. studied the effect of aqueous phase glycerol reforming conditions on the structure of Pt−Mo/C by in situ XAS. Using extended X-ray absorption fine structure (EXAFS), they identified the structure of the PtMo nanoparticles under reaction conditions and showed that the core was rich in Pt and the surface was rich in Mo and that Mo was partially oxidized. In addition, using X-ray absorption near edge structure (XANES) of adsorbed CO, they estimated the amount of Pt on the surface of the nanoparticles to be about 25%.[15]

We have recently reported that Pt/C activity and selectivity during aqueous phase reforming (APR) of glycerol was strongly affected by the addition of KOH. The catalyst activity increased dramatically; however, the selectivity toward C−C cleavage decreased.[16] In this paper, we report in situ X-ray absorption spectroscopy (XAS) results that correlate the Pt local coordination and electronic structure with the Pt/C catalyst

Special Issue: Operando and In Situ Studies of Catalysis

Received: July 27, 2012
Revised: September 20, 2012
Published: October 1, 2012

   dx.doi.org/10.1021/cs3005049 | ACS Catal. 2012, 2, 2387−2394

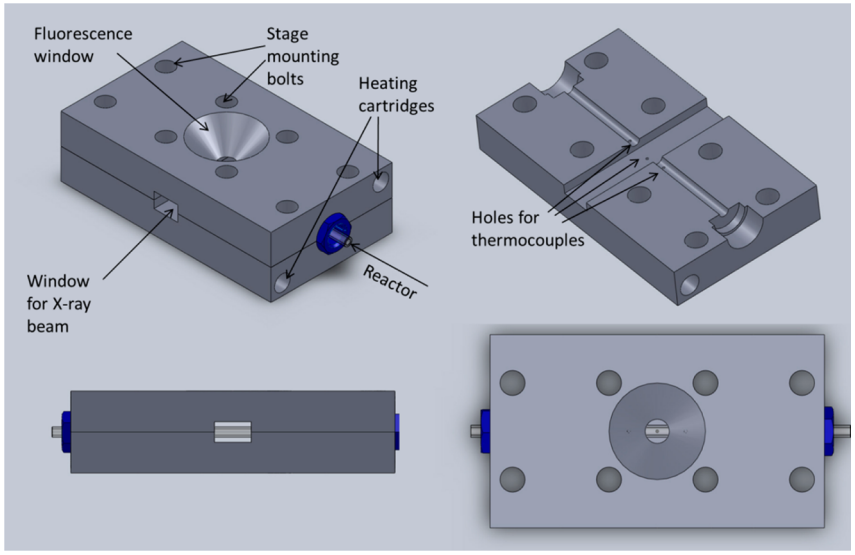

Figure 1. Schematic of the operando XAS cell.

activity and selectivity during APR of glycerol at pH ranging from 2 to 12. The spent catalysts were characterized by aberration corrected transmission electron microscopy to determine the effect of pH on the Pt average particle size and size distribution. We show that the solution pH (adjusted using HNO_3 or KOH) had a strong effect on the catalyst activity and selectivity. However, only HNO_3 (pH = 2) showed modification of the Pt electronic properties as evidenced by XANES. We show that, during glycerol APR, the electron density on Pt is higher at low pH (pH = 2.0) and that the selectivity to C−C cleavage is lower than at intermediate pH (pH = 5.5). KOH (pH =11.8) showed no measurable effect on the Pt electronic density by XANES, while the catalyst selectivity to C−C cleavage decreased compared with pH of 5.5. The effect of HNO_3 and KOH on the adsorbates during glycerol APR were estimated by ΔXANES and the effect on catalyst selectivity is discussed.

MATERIALS AND METHODS

Catalyst Synthesis. Three wt% Pt supported on high surface area activated carbon support (PICATAL, 1100 m^2/g, pore volume 0.42 mL/g) was prepared by incipient wetness. Specifically, 20 g of the dried carbon support was impregnated with a solution prepared by dissolving 1.24 g of Pt-$(NH_3)_4(NO_3)_2$ into 8.4 g of deionized water in a 30 mL glass vial, with shaking for at least 2 h prior to use. The impregnated sample was dried at 110 °C in air for 2 h and then calcined at 260 °C in air for 2 h with a ramp rate of 5 °C/min.

Transmission Electron Microscopy. The fresh and spent catalysts were characterized using aberration-corrected scanning transmission electron microscopy (STEM) with an FEI Titan microscope operated at 300 kV. The FEI Titan is equipped with CEOS GmbH double-hexapole aberration corrector for the probe-forming lens, which allows imaging with ∼0.1 nm resolution in scanning transmission electron microscopy (STEM) mode. The images were acquired in High Angle Annular Dark Field (HAADF) with an inner collection angle of 52 mrad. The TEM sample preparation involved mounting of powder samples on copper grids covered with lacey carbon support film.

EXAFS in Situ Setup and Data Analysis. The catalysts were characterized using an in-house built in situ X-ray absorption spectroscopy (XAS) cell. A schematic of the cell is shown in Figure 1, and detailed drawings of the cell are available in the Supporting Information. The in situ XAS reaction cell is capable of probing working catalysts under aqueous phase reactions under reaction conditions up to 1100 psig and 400 °C. The cell consists of the flow reactor and the cell body which is fabricated out of stainless steel and heated by resistive heating cartridges. An X-ray window (1 cm horizontal × 0.5 cm vertical) allows for measurements in transmission mode. In addition, the cell has a fluorescence window (0.25″ conical hole) perpendicular to the beam path. All the gas/liquid lines are 1/16 in. o.d. (500 μm i.d.) and the valves from Upchurch Scientific have a low internal volume (12 μL or less). The small cell dimensions and the low volume of the ancillaries make the whole system compact and easy to assemble even in the confines of small hutches. The whole system typically takes about 1 h to assemble before being ready to start acquiring scans.

The flow reactor (shown in Figure 1 inside the cell) consisted of either a 1.37 mm o.d. (1.0 mm i.d.) quartz or 3.1 mm o.d. (1.45 mm i.d.) glassy carbon tube (Tokai Carbon) where the catalyst bed is kept in place using quartz wool on both sides. The tubes were connected to the rest of the system via standard Swagelok fittings using graphite ferrules (450 °C temperature rating). The 1/8 in. Swagelok nut used for the connection was welded to the bottom half of the cell to eliminate any mechanical stress on the reactors. We used the Barlow formula to estimate the tubes burst pressure, $P_{max} = (2 \times t_{wall} \times S)/d$, where, t_{wall} is the wall thickness, S is the material yield strength, and d is the tube outer diameter (inch). The yield strength for both quartz and glassy carbon is about 20,000 psi; however, we used a safety factor of 10 in our calculations. The estimated maximum pressure using a safety factor of 10 was 590 and 1100 psi for the quartz and glassy carbon tubes, respectively. Experimentally, the quartz tube was tested up at 550 psig at 225 °C while the glassy carbon tube was tested up to 700 psig and 225 °C without failure. At atmospheric pressure the glassy carbon tube was tested at temperatures up to 700 °C

dx.doi.org/10.1021/cs3005049 | ACS Catal. 2012, 2, 2387−2394

without any signs of material deterioration based on pressure test (700 psig at 225 °C) conducted afterward.

A charge of 14 mg of catalyst (60−100 mesh) was packed into the reactor, and quartz wool was placed on either side of the catalyst to maintain the catalyst particles in place during experiments. The reaction temperature was controlled within ±1 °C, measured on the external tube wall, using a Watlow temperature controller. The liquid products were condensed downstream of the back pressure regulator in a condenser kept at room temperature. We used a mixed-phase backpressure regulator (Upchurch) capable of maintaining a stable pressure with small amounts of gas in the liquid flow. In addition, the small lines, low internal volume valves allow for fast system equilibration when changing feed flow rate or feed composition. The gas products were analyzed using online mass spectrometry to measure the reaction kinetics while probing the catalyst structure using XAS. The XAS measurements were performed at beamline X-18B at the National Synchrotron Light Source (NSLS) operated by the Synchrotron Catalysis Consortium (SCC) at Brookhaven National Laboratory. Some experiments were also conducted at beamline 20-BM-B at the Advanced Photon Source (APS) at Argonne National Laboratory. At the Pt L_3 edge the measured absorption from the tube walls was ~67% for the quartz tube and ~37% for the glassy carbon tube. The measured Pt absorption edge step for 3%Pt/C was about 0.13 in the quartz tube and 0.22 in the glassy carbon tube.

XANES and EXAFS data processing and analysis were performed using Athena and Artemis programs of the IFEFFIT data analysis package.[17,18] Five scans were collected under each condition and merged after alignment using Pt foil spectrum collected simultaneously for each scan. $\chi(k)$ (where k is the photoelectron wavenumber) was obtained by subtracting smooth atomic background from the normalized absorption coefficient using the AUTOBK code. The theoretical EXAFS signal was constructed using the FEFF6 code[19] and fitted to the data in r-space using the Artemis program of the IFEFFIT package. The spectra were fitted in r-space by varying the coordination number of the single scattering Pt−Pt path, N_{Pt-Pt}, the bond length disorder (Debye−Waller factor), σ^2, the effective Pt−Pt scattering length (R_{Pt-Pt}), and the correction to the threshold energy, ΔE_0. S_0^2 (the passive electron reduction factor) was obtained by first analyzing the spectrum for a Pt foil, and the best fit value (0.86) was fixed during the fitting of the Pt/C catalyst samples. The k-range used for Fourier Transform of the $\chi(k)$ was 2.5−13 $Å^{-1}$ and the r-range for fitting was 1.8−3.3 Å.

ΔXANES was obtained by subtracting the XANES spectrum for the catalyst under He flow at 225 °C from the spectra under reaction conditions and in the presence of different adsorbates at the same temperature. For the XANES spectrum under He, the spent catalyst was reduced at 320 °C in a flow of 100% H_2 for 2 h followed by flushing in He flow at 320 °C for 30 min and then at 340 °C for 10 min. After flushing with He the catalyst was cooled down to 225 °C in He where the XANES spectrum under He was collected. The XANES spectra under H_2 were collected on the fresh and spent catalyst. Under CO, XANES was only collected on the spent catalyst after reduction at 320 °C in 100% H_2 for 2 h (then flushing with He as described above). All gas flows were maintained at 20 sccm.

APR Experimental Setup. The catalyst activity and selectivity for glycerol APR were measured in a system similar to the in situ XAS system described above. The reactor consisted of 1/8 in. o.d. stainless steel tube with an inner diameter of 1.5 mm. The reactor was placed in a stainless steel block with a cavity of 1/8 in., and the s.s. block was heated using resistive heating cartridges. The block and reactor were mounted in a horizontal position. The reaction temperature was controlled within ±1 °C, measured on the external tube wall, using a Watlow temperature controller. A thermocouple at the inlet of the catalyst bed measured no more than a 1 °C temperature difference from the tube wall. At the outlet of the reactor a N_2 flow of 10 sccm was mixed with the products to serve as an internal analytical standard. The liquid products were condensed downstream of the back pressure regulator in a condenser kept at 0 °C. We used a mixed-phase backpressure regulator (Equilibar) capable of maintaining a stable pressure with a gas−liquid flow. This allowed the system to equilibrate faster since we avoided the long time needed to flush/pressurize the condenser if it was kept on the high pressure side (upstream of the backpressure regulator). The liquid products were collected for 2 h after analysis of the gas products to ensure that the liquid and gas analysis were performed at the same time on stream. Gas product analysis was carried out using a micro gas chromatograph (Agilent Micro GC 3000C) equipped with four channels, one molecular sieve 5A column, one Plot Q column, and two OV-1 columns. The liquid products were analyzed with a Waters high performance liquid chromatograph (HPLC). A Bio-Rad Aminex HPX-87H ion exclusion column (300 mm × 7.8 mm) was used for analyte separation. A 0.005 M H_2SO_4 aqueous solution was used as eluent for this analysis at a flow rate of 0.55 mL/min. Carbon balance was typically greater than 95%.

A charge of 50 mg catalyst (60−100 mesh) was packed into the reactor, and quartz wool was placed on either side of the catalyst to maintain the catalyst particles in place during experiments. Prior to the reaction test, the catalyst was reduced at 320 °C for 2 h in pure H_2 (20 sccm) at atmospheric pressure and cooled down to room temperature. After purging the system with N_2 for 30 min, the backpressure regulator was set at the reaction pressure (425 psig), the aqueous feed solution comprising 10% glycerol (by weight) was introduced using an HPLC digital pump (Series III) at the desired feed rate, and heating of the catalyst bed was initiated. When the reactor reached the reaction temperature of 225 °C, the internal standard N_2 flow (mixed with the outlet of the reactor) was set at 10 sccm. The system was allowed to stabilize for about 3 h at the start of the experiment and after changing the feed composition prior to analysis of the reaction products. The glycerol conversion was determined by

$$\text{Conversion} = \text{moles glycerol reacted}/\text{moles glycerol fed}$$

$$\text{Conversion to gas phase} = \text{moles carbon in the gas phase}/(3 \times \text{moles glycerol fed})$$

The selectivity to H_2 is defined based on the reforming of glycerol to H_2 and CO_2

$$C_3H_8O_3 + 3H_2O \rightarrow 7H_2 + 3CO_2 \text{ as } S_{H2} = \frac{\text{moles } H_2 \text{ produced}}{7 \times \text{moles glycerol reacted}}$$

Similarly,

$$S_{CO2} = \frac{\text{moles } CO_2 \text{ produced}}{3 \times \text{moles glycerol reacted}}$$

dx.doi.org/10.1021/cs3005049 | ACS Catal. 2012, 2, 2387−2394

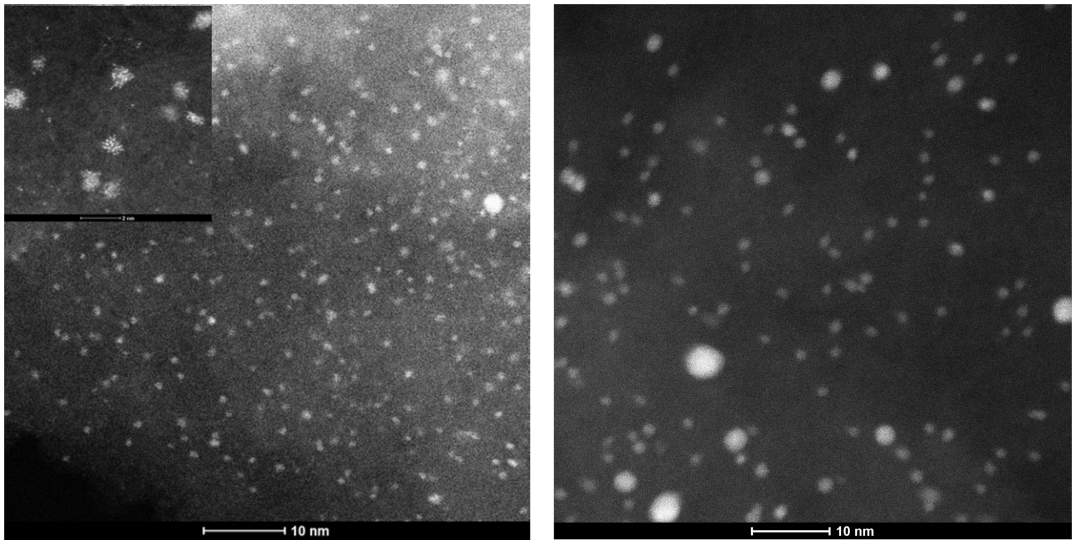

Figure 2. Representative STEM images of the fresh (left) and spent, pH = 11.8 (right) 3% Pt/C. The scale bar is equal to 10 nm for both images. The inset in the left image shows a higher magnification image for the fresh catalyst, the scale bar equals 2 nm in the inset.

The selectivity of the catalyst is also expressed in terms of the C−O/C−C ratio which is defined as the number of C−O bonds cleaved divided by the number of C−C bonds cleaved:[20]

$$\frac{\text{C}-\text{O}}{\text{C}-\text{C}} = \left(\sum_i \text{moles of dehydrated product}_i \times \text{dehydration steps to reach product}_i \right) / \text{moles of CO}_2$$

The C−O/C−C ratio is an indicator for the dehydration to decarbonylation selectivity of the catalyst which simplifies the comparison between the catalyst under the different conditions.

RESULTS AND DISCUSSION

TEM. Figure 2 shows representative STEM images of the fresh and spent 3%Pt/C catalyst, and Figure 3 shows the particle size distribution for the fresh and spent catalysts. It can be seen that the fresh catalyst had many small particles, clusters, and single atoms (a higher magnification image is provided in the Supporting Information). The APR reaction conditions resulted in sintering of the Pt nanoparticles. No single atoms were observed on the spent catalyst, and the number of small clusters was significantly lower than the fresh catalyst. Figure 3 shows that the particle size distribution for the two spent catalysts (at different pH, 2 and 11.8) was very similar. The particle size distributions in Figure 3 show that while APR reactions result in sintering of the Pt nanoparticles, the solution pH does not appear to affect the Pt particle size. The number average particle size increased from 1.0 ± 0.6 for the fresh catalyst to 2.3 ± 1.2 and 2.1 ± 1.2 for the spent catalyst at pH of 2 and 11.8, respectively. Figure 3 also shows that particles much larger (as large as 15 nm) than the number average (2.1−2.3 nm) were observed in the spent catalysts.

Glycerol APR. The effect of pH on the activity and selectivity of 3% Pt/C during glycerol APR is shown in Table 1 (the identity of liquid products and their selectivity are listed in Supporting Information, Table S1). It can be seen that even without the addition of acid or base, the selectivity to H_2 and

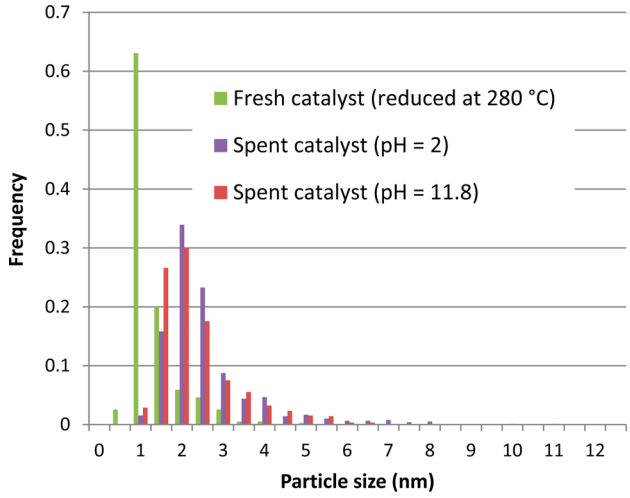

Figure 3. Particle size distribution for the fresh (reduced at 320 °C) and spent 3% Pt/C catalyst. Green: fresh catalyst, purple: spent (pH = 2), red: spent (pH = 11.8). Reaction conditions are the same as listed for Table 1. The particle size distribution consists of at least 500 particles for each catalyst.

Table 1. Conversion and Selectivity for Glycerol APR at 225 °C and 420 psig, WHSV = 6 $g_{glycerol}/g_{catalyst}/h$

	10% glycerol	10% glycerol + 0.018 M KOH	10% glycerol + 0.01 M HNO_3
pH	5.5	11.8	2
conversion (%)	9.7%	18.5%	18.5%
conversion to gas phase (%)	5.3%	5.4%	6.3%
H_2 selectivity (%)	35.5%	15.2%	11.0%
CO_2 selectivity (%)	46.7%	29.0%	28.9%
C−O/C−C cleavage	0.45	0.72	0.84
H_2/CO_2 ratio	1.79	1.23	1.03

CO_2 was low on Pt/C. This is reflected in the C−O/C−C ratio of 0.45, which shows that for every 10 C−C bonds broken there were about 4.5 C−O bonds broken. Wawrzetz et al.

dx.doi.org/10.1021/cs3005049 | ACS Catal. 2012, 2, 2387−2394

Table 2. EXAFS Fitting Results for the 3%Pt/C Catalyst at the Pt L_3 Edge[a]

condition	N_{Pt-Pt}	σ^2 (Å^2)	R_{Pt-Pt} (Å)	ΔE_0 (eV)	d_{avg} (STEM)
H_2 before reaction[b]	7.2(5)	0.013(3)	2.730(6)	5.3 (6)	1.0 ± 0.6
H_2 after reaction[b]	9.1(5)	0.0093(4)	2.740(4)	6.3(4)	
CO after reaction[b]	9.4(5)	0.0106(5)	2.753(4)	7.3(4)	
APR, pH = 5.5	9.5(9)	0.0098(7)	2.752(6)	6.1(8)	
APR, pH = 2	9.7(6)	0.0096(5)	2.752(6)	7.3 (9)	2.3 ± 1.2
APR, pH = 5.5[c]	9.3(9)	0.0103(9)	2.752(6)	6.6(8)	
APR, pH = 11.8[c]	9.3(8)	0.0104(7)	2.753(6)	6.6(7)	2.1 ± 1.2

[a]Average particle size obtained by STEM is also included. The average particle size was obtanied by measuring over 500 particles from several images of different areas on the grid. All EXAFS spectra were collected at 225 °C. The reaction conditions for glycerol APR were 225 °C and 440 psig, WHSV = 89 $g_{glycerol}/g_{catalyst}$/h. The numbers in parentheses indicate the statistical error in the most significant digit obtained from the fit in Artemis (e.g. 7.2(5) ≡ 7.2 ± 0.5). [b]The catalyst was reduced under 100% H_2 flow for 2 h at 320 °C (1 atm) prior to collection of the EXAFS spectra at 225 °C. For EXAFS of 3%Pt/C with adsorbed CO, the sample was flushed with He at 340 °C after reduction in H_2 at 320 °C then cooled down to 225 °C before switching the flow to 3% CO in He. [c]Separate experiment using a fresh aliquot of the 3% Pt/C catalyst starting with pH 5.5 and then switching to pH 11.8.

reported significant dehydration of glycerol on Pt black during APR of glycerol. The authors hypothesized that Pt could act as a solid acid through the adsorbed hydroxyl groups.[21] Our results also confirm that Pt can act as a solid acid during the APR reaction conditions, as seen from the (C−O/C−C) ratio in Table 1.

The addition of 0.018 M KOH (pH = 11.8) resulted in higher glycerol conversion while the conversion to gas phase products was not affected. The higher conversion without an increase in gas products is due to a higher selectivity to dehydrated products which is reflected in the lower CO_2 and H_2 selectivities and higher C−O/C−C ratio. For every C−O bond broken, a H_2 molecule is consumed for the hydrogenation of the dehydrated product, and this can be seen in the lower H_2/CO_2 ratio compared to that without KOH.

HNO_3 addition (0.01 M, pH = 2) also showed an increase in glycerol conversion and lower selectivity to H_2 and CO_2. In addition, the selectivity to H_2 was affected by HNO_3 more than by KOH which can be seen in the lower H_2/CO_2 and higher C−O/C−C ratios of 1.03 and 0.84 compared to 1.23 and 0.72 under KOH. Blank experiments (not shown) conducted with and without the carbon support under the same conditions, Table 1, and with a simulated products mixture (see Supporting Information, Table S1 for the products detected) showed less than 0.5% glycerol conversion (less than 0.1% conversion to gas phase) by KOH or HNO_3. Therefore, in the case of glycerol APR on Pt/C, we believe that the effect of pH on the catalyst activity and selectivity is mainly due to the interaction of KOH or HNO_3 with Pt and/or the adsorbates on the Pt surface and not due to homogeneous chemistry of glycerol catalyzed by the acid or base. The catalyst activity and selectivity will be further discussed in connection with the XAS results in the next section.

It should be mentioned that our results showed that the effect of both HNO_3 and KOH was reversible. The catalyst activity and selectivity at pH 5.5 was similar before and after the tests at pH 2 and 11.8 (the system was flushed for 3 h with 10% glycerol, pH = 5.5, to remove either KOH or HNO_3 from the reactor). This suggests that KOH and HNO_3 do not affect the catalyst structure permanently and that the sintering of Pt nanoparticles observed by TEM occurs under APR reaction conditions independent of pH. This is also confirmed by the in situ EXAFS results at the different pH presented below.

In Situ XAS. The results of the EXAFS fits for the fresh catalyst, spent catalyst and under APR reaction conditions are shown in Table 2. Supporting Information, Figures S1 and S2 show examples of the data quality in *k*-space as well as the fit quality in r-space. The average Pt first shell coordination number increased from 7.2 to 9.1 after exposure to the glycerol APR reaction conditions. A coordination number of 7.2 and 9.1 correspond to an average (volume average) hemispherical particle size of about 1.5 and 2.6 nm, respectively.[22] The increase in coordination number is consistent with the sintering seen in the STEM images in Figure 2 and the particle size distributions in Figure 3. Also, consistent with the increase in coordination number, an increase in the Pt−Pt bond length and a decrease in the Debye−Waller factor was observed, as seen in Table 2. The EXAFS spectra for the low and high pH were collected during separate experiments using two different catalyst aliquots from the same batch, and we collected spectra on the catalyst under pH = 5.5 in both experiments. The results in Table 2 show that the fitting results are reproducible from two independent experiments. The pH of the reaction medium does not appear to affect the Pt coordination number, which is in agreement with the similar particle size obtained by TEM on the spent catalysts. Since the solution pH has little effect on the size of Pt nanoparticles during glycerol APR, comparison of XANES spectra will provide insights on the interaction of the acid and base with the Pt surface and their effect on the adsorbates and Pt electron density.

Figure 4 shows the XANES spectra during glycerol APR under different pH. It can be clearly seen that KOH has a minimal effect on the white line intensity while HNO_3 results in a lower white line intensity. It has been reported that, under the same atmosphere, the white line intensity is affected by the Pt particle size.[23] This can be seen in the XANES spectra for the fresh and spent catalysts under 100% H_2 shown in Figure 5. However, the increase in particle size is also expected to result in a shift of the edge energy as seen in Figure 5 in agreement with reports in the literature on Pt/Al_2O_3.[23,24] In addition, the effect of pH (for both KOH and HNO_3) on the catalyst activity and selectivity was reversible and since the particle size from TEM and the coordination numbers from EXAFS are similar at different pH, the changes in XANES (Figure 4) are not due to a change in particle size. Therefore, the lower white line intensity at low pH (Figure 4) is due to a higher electron density on Pt. The higher electron density could be due to HNO_3 (for example NO_3^-) directly interacting with the Pt surface, or indirectly by HNO_3 interacting either with the adsorbates and affecting their surface coverage or with the carbon support.

dx.doi.org/10.1021/cs3005049 | ACS Catal. 2012, 2, 2387−2394

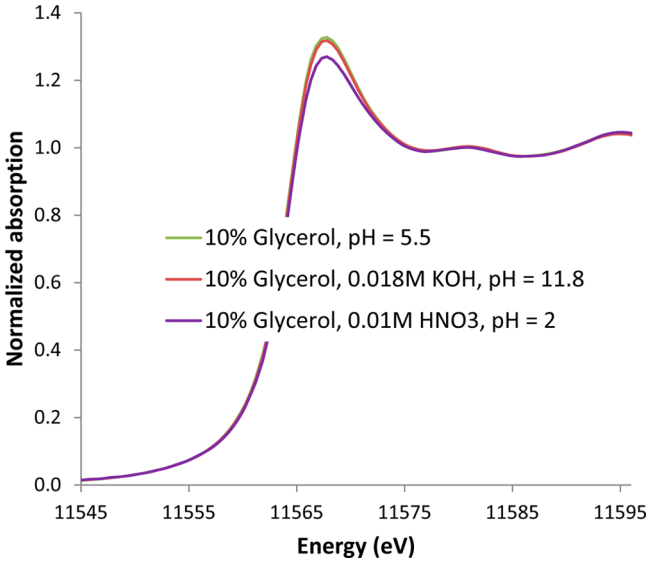

Figure 4. Pt L_3 XANES spectra of the 3%Pt/C under glycerol APR at 225 °C and 440 psig, WHSV = 89 $g_{glycerol}/g_{catalyst}/h$. Green: 10% glycerol, pH = 5.5; purple: 10% glycerol +0.01 M HNO_3, pH = 2; red: 10% glycerol +0.018 M KOH3, pH = 11.8.

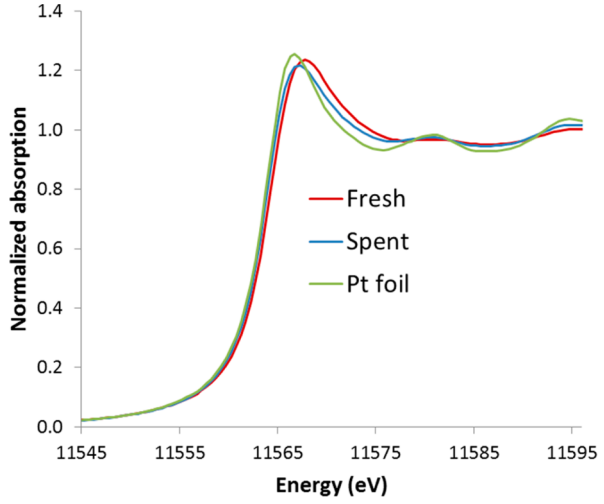

Figure 5. Pt L_3 XANES spectra of the Pt foil (green) and the fresh (red) and spent (blue) 3%Pt/C catalyst under 100% H_2 at 225 °C (1 atm). The spent catalyst was exposed to glycerol APR (pH = 5.5) at 225 °C and 440 psig, WHSV = 89 $g_{glycerol}/g_{catalyst}/h$.

Using ATR-FTIR, Ebbesen et al. showed that pH affected the frequency of linearly adsorbed CO on Pt/Al_2O_3 at room temperature.[14] Higher pH resulted in lower frequency of the linearly adsorbed CO while low pH resulted in the opposite effect. The authors attributed the effect of pH on the frequency of adsorbed CO to a change in the potential of the Pt surface caused by the solution pH.[14] However, the frequency of adsorbed CO on Pt observed by IR can be affected by factors other than the direct bonding of CO with Pt, such as CO coverage as well as interaction of the solvent with the adsorbed CO (for example through H bonding).[14] On the other hand, Pt L_3 XANES is very sensitive to the density of unoccupied d-states and is a more direct measure of the electron density on Pt where the white line intensity is proportional to the d-electron vacancies.[25,26] The dependence of white line intensity and position of the L_3 absorption edge on d-electron vacancies has been used to understand the effect of Pt nanoparticle size and interaction with support and adsorbates[23,24] and for estimating the coverage of adsorbates under reaction conditions.[27]

Figure 6 shows the Pt L_3 ΔXANES for the Pt/C catalyst during glycerol APR compared to adsorbed H_2 and CO at the same reaction temperature. XANES under water at 225 °C and 440 psig was collected on the catalyst after adsorption of H_2 without flushing with He; however, the water did not completely displace the preadsorbed H_2, and the ΔXANES spectrum resembled that of H_2 at lower coverage. Since CO and H_2 adsorption are much stronger than that of water, the water coverage during APR is expected to be very small. It can be seen that the ΔXANES during glycerol APR at pH = 5.5 looks very similar to that of CO. This is also consistent with the results in Table 2 showing that under APR reaction conditions, the Pt−Pt coordination number, Debye−Waller factor, and Pt−Pt bond length are very similar to those under CO at the same temperature.

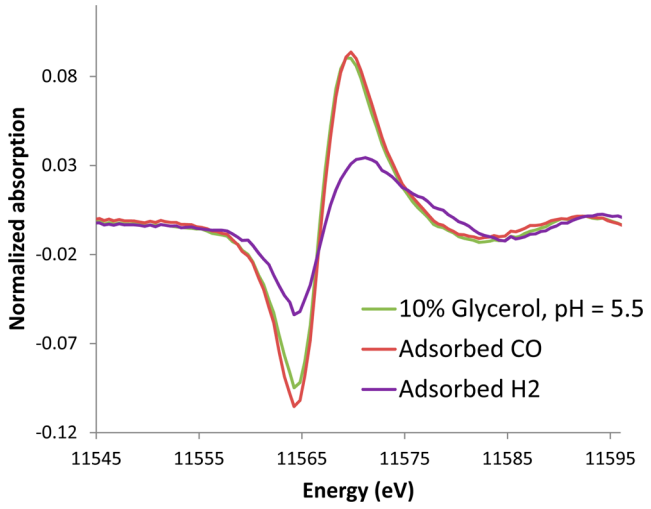

Figure 6. Pt L_3 ΔXANES spectra of the 3%Pt/C under glycerol APR (pH = 5.5) at 225 °C and 440 psig, WHSV = 89 $g_{glycerol}/g_{catalyst}/h$ (green), 3% CO in He at 225 °C and 1 atm (red) and under 100% H_2 at 225 °C and 1 atm (purple). The adsorbed H_2 and CO measurements were collected on the spent catalyst after reduction in 100% H_2 at 320 °C for 2 h then flushing with He at 340 °C for 30 min.

Figure 7 shows a comparison of the ΔXANES spectra during glycerol APR under different pH. The spectra for pH 5.5 and 11.8 are almost identical while the spectrum for pH = 2 looks different. The spectra were reproducible and the linear combination fit of CO and H_2 for glycerol APR at pH 5.5 and 11.8 shows that CO coverage was about about 93 and 95% of the coverage under a flow of 3% CO in He at 225 °C, repectively. The H_2 coverage during glycerol APR at pH 5.5 and 11.8 was only about 2−3% of that under 100% H_2 flow at 225 °C. The ΔXANES spectrum during glycerol APR at pH 2 showed a much lower CO coverage of 68% and required a H_2 coverage of 53% to be able to fit the spectrum (coverages are relative to that of CO and H_2 at 225 °C, respectively, and not absolute coverage on Pt). It should be noted that the goodness of fit was lower for the spectrum at pH = 2 (Supporting Information, Figure S4). The ΔXANES spectra and linear combination fits using CO and H_2 show that HNO_3 has a strong influence on the adsorbates. Also, from the lower quality

dx.doi.org/10.1021/cs3005049 | ACS Catal. 2012, 2, 2387−2394

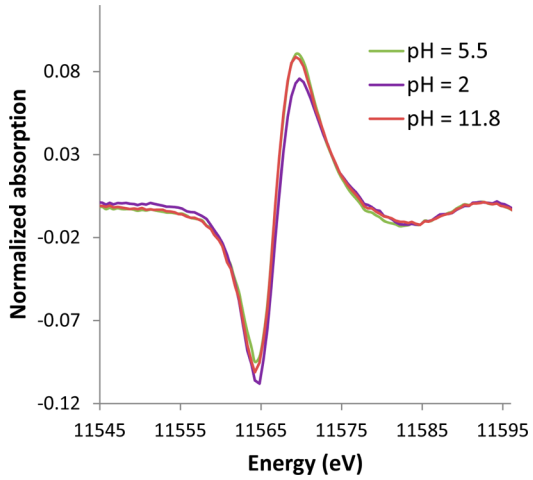

Figure 7. Pt L_3 ΔXANES spectra of the 3%Pt/C under glycerol APR at 225 °C and 440 psig, WHSV = 89 $g_{glycerol}/g_{catalyst}/h$. Green: 10% glycerol, pH = 5.5; purple: 10% glycerol +0.01 M HNO_3, pH = 2; red: 10% glycerol +0.018 M KOH, pH = 11.8.

of the ΔXANES fit at pH = 2 (Supporting Information, Figure S4), CO and H_2 might not be the only adsorbates present on the Pt surface under the acidic conditions. The change in coverage of CO and H_2 and/or the presence of other adsorbates would be responsible for the higher Pt electron density. A higher H_2 coverage on Pt could explain the higher C−O hydrogenolysis activity (higher C−O/C−C and lower H_2/CO_2 in Table 1) at the low pH but this needs further study to be confirmed. We believe that the effect of HNO_3 on the adsorbates and the catalyst selectivity is due to either interaction of NO_3^- with the Pt surface or with adsorbed CO (lowering the CO binding energy) or a combination of both. It is surprising that the Pt electron density was only affected by HNO_3 at the low pH and not by KOH at the high pH, especially that the glycerol conversion and C−O cleavage activity increased in both cases. The effect of KOH on the activity and selectivity could be explained through interaction with the adsorbed reaction intermediates on the surface of Pt. While glycerol and the liquid reaction products showed negligible homogeneous reaction with KOH and HNO_3 (in blank experiments with and without the carbon support), other intermediates (especially aldehydes) could react with KOH or HNO_3. It was reported by Maris and Davis that addition of base (0.01 M NaOH) increased the activity of Pt/C for the hydrogenolysis of glycerol and increased the ratio of propylene glycol to ethylene glycol in the products.[28] They attributed the increased propylene glycol formation to base catalyzed dehydration of glyceraldehyde to pyruvaldehyde followed by metal catalyzed hydrogenation. Their results seem to suggest that a metal site is required for the initial dehydrogenation of glycerol to glyceraldehyde[28] which is consistent with our blank experiments. Base addition was also reported to increase 2-propanol dehydrogenation activity on Pt/C.[29] Base induced higher dehydrogenation activity on Pt coupled with base catalyzed dehydration of aldehydes could explain our higher glycerol conversion at pH = 11.8 as well as the higher C−O/C−C selectivity (Table 1) compared with that at pH = 5.5. This can also be seen in the higher selectivity to propylene glycol and ethanol at pH = 11.8 compared with pH = 5.5 (see Supporting Information, Table S1). It is unclear whether the reaction of KOH with the aldehydes occurs while the aldehydes are still adsorbed on Pt or after desorption. However, because of the high reactivity of aldehydes under glycerol hydrogenolysis and APR reaction conditions,[28] we suspect that they react with KOH in the adsorbed state. Enhanced dehydrogenation activity of glycerol in the homogeneous phase by KOH is highly unlikely since glycerol showed negligible reaction with KOH in the absence of Pt. The interaction of KOH with adsorbed intermediates appears to have negligible effect on the most abundant intermediates, CO and H_2, (see Figure 7) which dominate the ΔXANES signal under reaction conditions. Another indication that KOH interacts more strongly than HNO_3 with the adsorbed intermediates (especially aldehydes) is the increased acids formation by KOH compared with HNO_3 during glycerol APR (Supporting Information, Table S1).

CONCLUSIONS

We have reported in situ X-ray absorption spectroscopy (XAS) results on correlating the Pt local coordination and electronic structure with the Pt/C catalyst activity and selectivity during aqueous reforming of glycerol at different pH. The Pt nanoparticles undergo sintering when exposed to the APR reaction conditions as confirmed by both TEM and in situ EXAFS. The catalyst activity and selectivity was strongly influenced by the pH of the reaction medium. XANES measurements during glycerol APR showed that KOH addition (pH = 11.8) had a negligible effect on the electron density of Pt while HNO_3 addition (pH = 2.0) resulted in a higher electron density on Pt. The selectivity to C−O cleavage increased in the presence of acid or base; however, it was higher in the presence of HNO_3. The change in selectivity at pH = 11.8 is believed to be due to interaction of KOH with adsorbed reaction intermediates on Pt, such as aldehydes. ΔXANES measurements under reaction conditions compared to adsorbed CO and H_2 suggest that HNO_3 resulted in increased H_2 coverage and a decrease in CO coverage on Pt. We attribute the change in coverage and higher C−O bond cleavage selectivity at pH = 2 to either the direct interaction of HNO_3 with CO and/or modification of Pt by HNO_3.

ASSOCIATED CONTENT

Supporting Information

Figures showing the data quality and fits, results for the glycerol APR blank experiments, and the drawings of the XAS cell. This material is available free of charge via the Internet at http://pubs.acs.org.

AUTHOR INFORMATION

Corresponding Author

*E-mail: ayman.karim@pnnl.gov.

Funding

The authors acknowledge financial support from the U.S. Department of Energy, Office of Energy Efficiency and Renewable Energy and from the National Advanced Biofuels Consortium, which is funded by the Department of Energy's Office of Biomass Program with recovery act funds. The TEM experiments were carried out at the Environmental and Molecular Sciences Laboratory, a user facility of the Department of Energy, of the Pacific Northwest National Laboratory. Use of the National Synchrotron Light Source, Brookhaven National Laboratory, for the EXAFS experiments was supported by the U.S. Department of Energy, Office of Basic Energy Sciences (Grant DE-FG02-05ER15688).

Notes

The authors declare no competing financial interest.

■ ACKNOWLEDGMENTS

A.M.K. would like to thank Zhehao Wei and Dr. Junming Sun (Washington State University) and Dr. Nebojsa Marinkovic (University of Delaware) for their help and support during the XAS experiments and would like to thank Prof. Anatoly Frenkel (Yeshiva University) for numerous discussions and advice.

■ REFERENCES

(1) Huber, G. W.; Dale, B. E. *Sci. Am.* **2009**, *301*, 52.
(2) Kunkes, E. L.; Simonetti, D. A.; West, R. M.; Serrano-Ruiz, J. C.; Gartner, C. A.; Dumesic, J. A. *Science* **2008**, *322*, 417.
(3) Huber, G. W.; Iborra, S.; Corma, A. *Chem. Rev.* **2006**, *106*, 4044.
(4) Elliott, D. C.; Beckman, D.; Bridgwater, A. V.; Diebold, J. P.; Gevert, S. B.; Solantausta, Y. *Energy Fuels* **1991**, *5*, 399.
(5) Bridgwater, A. V. *Catal. Today* **1996**, *29*, 285.
(6) Bridgwater, A. V. *J. Anal. Appl. Pyrolysis* **1999**, *51*, 3.
(7) Bridgwater, A. V.; Peacocke, G. V. C. *Renewable Sustainable Energy Rev.* **2000**, *4*, 1.
(8) Bond, J. Q.; Alonso, D. M.; Wang, D.; West, R. M.; Dumesic, J. A. *Science* **2010**, *327*, 1110.
(9) Huber, G. W.; Chheda, J. N.; Barrett, C. J.; Dumesic, J. A. *Science* **2005**, *308*, 1446.
(10) Huber, G. W.; Shabaker, J. W.; Dumesic, J. A. *Science* **2003**, *300*, 2075.
(11) Serrano-Ruiz, J. C.; Dumesic, J. A. *Energy Environ. Sci.* **2011**, *4*, 83.
(12) Zhao, C.; Kou, Y.; Lemonidou, A. A.; Li, X. B.; Lercher, J. A. *Angew. Chem., Int. Ed.* **2009**, *48*, 3987.
(13) Carlos Serrano-Ruiz, J.; Dumesic, J. A. *Energy Environ. Sci.* **2011**, *4*, 83.
(14) Ebbesen, S. D.; Mojet, B. L.; Lefferts, L. *J. Catal.* **2007**, *246*, 66.
(15) Dietrich, P. J.; Lobo-Lapidus, R. J.; Wu, T.; Sumer, A.; Akatay, M. C.; Fingland, B. R.; Guo, N.; Dumesic, J. A.; Marshall, C. L.; Stach, E.; Jellinek, J.; Delgass, W. N.; Ribeiro, F. H.; Miller, J. T. *Top. Catal.* **2012**, *55*, 53.
(16) King, D. L.; Zhang, L.; Xia, G.; Karim, A. M.; Heldebrant, D. J.; Wang, X.; Peterson, T.; Wang, Y. *Appl. Catal., B* **2010**, *99*, 206.
(17) Ravel, B.; Newville, M. *J. Synchrotron Radiat.* **2005**, *12*, 537.
(18) Newville, M. *J. Synchrotron Radiat.* **2001**, *8*, 96.
(19) Zabinsky, S. I.; Rehr, J. J.; Ankudinov, A.; Albers, R. C.; Eller, M. J. *Phys. Rev. B* **1995**, *52*, 2995.
(20) Zhang, L.; Karim, A. M.; Engelhard, M. H.; Wei, Z.; King, D. L.; Wang, Y. *J. Catal.* **2012**, *287*, 37.
(21) Wawrzetz, A.; Peng, B.; Hrabar, A.; Jentys, A.; Lemonidou, A. A.; Lercher, J. A. *J. Catal.* **2010**, *269*, 411.
(22) Frenkel, A. I.; Hills, C. W.; Nuzzo, R. G. *J. Phys. Chem. B* **2001**, *105*, 12689.
(23) Lei, Y.; Jelic, J.; Nitsche, L.; Meyer, R.; Miller, J. *Top. Catal.* **2011**, *54*, 334.
(24) Sanchez, S. I.; Menard, L. D.; Bram, A.; Kang, J. H.; Small, M. W.; Nuzzo, R. G.; Frenkel, A. I. *J. Am. Chem. Soc.* **2009**, *131*, 7040.
(25) Lytle, F. W.; Greegor, R. B.; Marques, E. C.; Sandstrom, D. R.; Via, G. H.; Sinfelt, J. H. *J. Catal.* **1985**, *95*, 546.
(26) Mansour, A. N.; Cook, J. W.; Sayers, D. E. *J. Phys. Chem.* **1984**, *88*, 2330.
(27) Guo, N.; Fingland, B. R.; Williams, W. D.; Kispersky, V. F.; Jelic, J.; Delgass, W. N.; Ribeiro, F. H.; Meyer, R. J.; Miller, J. T. *Phys. Chem. Chem. Phys.* **2010**, *12*, 5678.
(28) Maris, E. P.; Davis, R. J. *J. Catal.* **2007**, *249*, 328.
(29) Ukisu, Y.; Miyadera, T. *React. Kinet. Catal. Lett.* **2004**, *81*, 305.